NJC

PAPER

View Article Online
View Journal | View Issue

Cite this: *New J. Chem.*, 2018, **42**, 18102

Mussel-inspired preparation of C_{60} nanoparticles as photo-driven DNA cleavage reagents†

Yihan Ma,* [a] Xiaoyan Zhang,[a] Yinjia Cheng,[a] Xiaosui Chen,[a] Yong Li*[b] and Aiqing Zhang[a]

Received 6th August 2018,
Accepted 30th September 2018

DOI: 10.1039/c8nj03970d

rsc.li/njc

Designing and constructing favorable water-dispersible fullerenes and their derivatives are of huge importance for biological applications addressing DNA-cleavage and photodynamic therapy (PDT). In the present work, a mild, green and facile synthetic approach for the preparation of C_{60} nanoparticles was developed for the first time *via* the combination of mussel-inspired chemistry and the Michael addition reaction. The resultant C_{60}–PDA–PEI nanoparticles were characterized by transmission electron microscopy (TEM), dynamic laser scattering (DLS), Fourier-transform infrared spectroscopy (FT-IR), Raman spectra, X-ray photoelectron spectra (XPS) and thermogravimetric analysis (TGA), demonstrating that the above two-step strategy allows easy access to the preparation of highly water-dispersible fullerene derivatives. Benefiting from their unique nanostructure, the versatile C_{60}–PDA–PEI nanoparticles display a uniform hydrodynamic size of 160 nm in water and efficient $^1O_2$ generation under irradiation. Furthermore, the good ability of cleaving DNA under visible light at a mass concentration of 62.5 ng μL^{-1} gives them high potential as PDT agents. The universal approach described in this work is capable of introducing many other functional molecules onto PDA-modified fullerenes, thus extending the possible applications of fullerene-based species in many fields of biotechnology and pharmaceutical chemistry.

Introduction

In the past few decades, the ready availability of fullerenes and their various derivatives has aroused considerable interest and exploration.[1–4] As a class of low-dimensional materials, fullerenes consist of sp^2 carbons, which form a highly symmetric cage with different sizes. Due to their outstanding opto-electronic, chemical and physiochemical properties, great research efforts have been devoted to a broad range of applications.[5–7] In particular, for bio-applications, fullerenes could be excited to their triplet state and efficiently produce reactive oxygen species (ROS) in the presence of irradiation and oxygen.[8] As a result, fullerenes are anticipated as promising photosensitizers to cleave DNA and further for photodynamic therapy (PDT).[9–11] Nevertheless, the hydrophobic nature of fullerenes results in unfavorable solubility in polar media, especially aqueous solutions, which is extremely challenging and critical for biological applications. In order to get rid of this defect, a number of methods have been developed to boost fullerene solubility in water.[12–14] In general, two strategies are adopted to obtain biocompatible fullerene-based materials: (1) the introduction of hydrophilic groups by chemical modification, such as hydroxyl,[15] carboxyl[16] and amino[17] or the conjugation of small hydrophilic molecules (saccharides[18] and peptides[19]) or polymers[20,21] *via* different linkers, and (2) taking advantage of a solubilizing agent to partially mask the fullerene surface, by the non-covalent encapsulation of soluble macromolecules[22] or host molecules (cyclodextrins[23] and liposomes[24]). Commonly, the preparation of C_{60} nanoparticles obtained by solvent exchange (THF[25] or toluene[26]) needs extra washing steps to remove the toxic byproducts. As for the host–guest complexes, previous results mentioned that the γ-CD_x·C_{60} complex must be handled carefully because of its instability, which limited its applications.[27] To date, much work has focused on a class of polyhydroxylated fullerenes (fullerenols), disclosing that the water-solubility and toxicity effects of fullerenols are dependent on the number of hydroxyl groups present on the carbon cage by different means.[15,28] Consequently, plenty of the previous methods may involve complicated reaction procedures, hazardous ingredients or harsh reaction conditions. Therefore, it is truly favorable to design and develop a facile and efficient synthesis route for highly water-dispersible fullerene derivatives, which could be biocompatible, low-cost and eco-friendly.

Inspired by the composition of adhesive proteins in mussels, Messersmith first proposed the fabrication of multifunctional coatings by the self-polymerization of dopamine in a weakly

[a] *College of Chemistry and Materials Science, South-Central University for Nationalities, Wuhan, 430074, China. E-mail: mayihan@iccas.ac.cn*
[b] *College of Life Sciences, South-Central University for Nationalities, Wuhan, 430074, China. E-mail: liyong081@mail.scuec.edu.cn*

† Electronic supplementary information (ESI) available: TEM images of C_{60}, DLS and ζ potential of C_{60}–PDA–PEI, XPS C 1s spectra and DTA curves of C_{60}, C_{60}–PDA and C_{60}–PDA–PEI. See DOI: 10.1039/c8nj03970d

alkaline solution.[29] The surface-adherent polydopamine (PDA), an emerging soft material, can be applied to the surface modification of almost any inorganic or organic material (noble metals, oxides, semiconductors, ceramics and polymers) regardless of its composition, shape and size.[30–33] More significantly, once the PDA thin film is formed, it can serve as a secondary reaction platform for covalent modification with other desired compounds. Thus, molecules containing amino or thiol groups, such as commercially available small molecules, peptides and polymers, could be immobilized onto PDA-modified materials through the Michael addition reaction.[31,34] Therefore, the universal adhesion capability and high reactivity of PDA imply the broad opportunities in directly modifying distinct substrates for multiple applications. Notably, considerable research efforts have been devoted to PDA-modified carbon nanomaterials.[35] The Wei and Zhang groups reported a series of work focusing on graphene oxide and carbon nanotubes fabricated *via* the above two-step method to obtain enhanced dispersibility, biocompatibility, applicability and capacity for multiple fields.[36–41] Additionally, Lee *et al.* demonstrated that PDA-coated GQDs (graphene quantum dots) could act as a long-term optical imaging agent with excellent stability of photoluminescence intensity.[42] In spite of this, fullerene, as a carbon-based nanomaterial, has rarely been related to the simple mussel-inspired chemistry. It is worthwhile introducing mussel-inspired PDA to fullerene as a strategy for functionalization of nanoparticles and studying their interconnection.

In this report, we describe the facile preparation and DNA photocleavage performance of C_{60}–PDA–PEI nanoparticles for the first time. C_{60} was first immobilized by PDA *via* the self-polymerization of dopamine, then hydrophilic polymer PEI was conjugated to the PDA-coated C_{60} through the Michael addition reaction (Scheme 1). A variety of characterization techniques was employed to verify the successful synthesis of the resultant C_{60}–PDA–PEI nanoparticles. At last, the versatile C_{60}–PDA–PEI nanoparticles with efficient $^1O_2$ generation in aqueous media can completely cleave closed supercoiled DNA to nicked DNA under visible light irradiation.

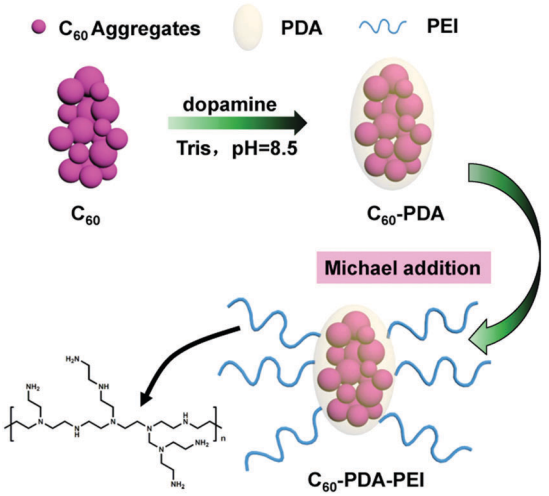

Scheme 1 Schematic representation of the preparation of C_{60}–PDA–PEI *via* the combination of mussel-inspired chemistry and the Michael addition reaction.

Experimental

Materials and instrumentation

All of the chemicals were obtained from commercial sources and used directly without further purification. C_{60} was obtained from the Institute of Chemistry, Chinese Academy of Sciences (Beijing, China). Tris-(hydroxymethyl) aminomethane (Tris), polyethyleneimine (PEI, M_n = 600), 2,2,6,6-tetramethyl-4-piperidone (TEMP) and dopamine hydrochloride were purchased from Aladdin Reagent Inc. (Shanghai, China). Ethylenediaminetetraacetic acid (EDTA) and ethidium bromide were purchased from Sigma, and pSP72 plasmid DNA was purchased from Promega. 6× gel loading buffer was purchased from CoWin Biosciences. Milli-Q purified water (18.2 MΩ) was used to prepare all of the solutions. The hydrodynamic size distribution and zeta potential of C_{60}–PDA–PEI nanoparticles in water were determined on a Zetasizer Nano ZSP instrument (DLS). Transmission electron microscopy (TEM) images were obtained using a Tecnai G^2 20 S-TWIN microscope and adding a drop of the nanoparticle ethanol suspension onto a carbon-coated copper grid to prepare the TEM samples. Fourier transform infrared (FT-IR) spectra were recorded using a Thermo Nexus470 spectrometer. Raman spectra were analysed using a LabRAM HR800 spectrometer with a 532 nm excitation wavelength. X-ray photoelectron spectroscopy (XPS) was performed on a VG ESCALab220i-XL spectrometer equipped with an Al Kα X-ray source (1486.6 eV) and the binding energies were internally calibrated by referencing to the C 1s peak of a carbon contaminant at 284.6 eV. Thermogravimetric analysis (TGA) was conducted on a TA instrument (Shimadzu DTG-60H) with a heating rate of 10 °C min^{-1} under a N_2 atmosphere. Electron spin resonance (ESR) spectroscopy was performed on a Bruker ELEXSYSE 500 ESR spectrometer at 298 K.

Preparation of C_{60}–PDA

In brief, 100 mg of C_{60} was dispersed in 30 mL of Tris buffer solution (pH = 8.5, 10 mM) with the aid of sonication for 20 minutes. Then, 200 mg of dopamine hydrochloride was directly added into the above solution. After that, the mixture was stirred vigorously at room temperature for 10 h and then separated by centrifuging at 8000 rpm for 10 min. The obtained C_{60}–PDA was washed repeatedly with distilled water and ethanol until the upper solution was clear and dried under vacuum at 40 °C for 12 h.

Preparation of C_{60}–PDA–PEI

50 mg of C_{60}–PDA and 100 mg of polyethyleneimine (PEI) were added into 25 mL of NaOH aqueous solution (0.1 M) and then stirred for 12 h at room temperature. The as-synthesized C_{60}–PDA–PEI nanoparticles in a red-brown aqueous solution were purified by filtering through a 0.22 μm membrane filter and dialyzed against ultrapure water with a porous cellulose

bag (molecular weight cut-off 3500 Da) for 3 days. Finally, the products inside the dialysis bag were collected by freeze drying.

Evaluation of $^1O_2$ generation by ESR spectroscopy

$^1O_2$ generated under visible light irradiation was detected by the ESR spin-trapping method. 25 μL of TEMP (30 mM) as the spin-trapping reagent and 25 μL of C_{60}–PDA–PEI (0.5 mg mL^{-1}) were mixed well under aerobic conditions. Then, the above solution was irradiated by a 50 mW cm^{-2} photoreflector at 298 K for 10 min and at once subjected to ESR measurements. The singlet oxygen generated by irradiation was immediately captured by 2,2,6,6-tetramethyl-4-piperidone (TEMP) to form TEMPO, which could be detected by ESR spectroscopy with the corresponding signal.

Examination of DNA-cleaving activity

To examine the DNA-cleaving activity of the as-prepared PDA–PEI–C_{60}, 2.5 μL of pSP72 plasmids (50 ng μL^{-1}) was mixed with an equal volume of different concentrations of PDA–PEI–C_{60} (125, 62.5, 31.25, 15.63, 7.82 and 3.91 ng μL^{-1}). For the blank control, PDA–PEI–C_{60} was absent, and 2.5 μL of ultrapure water was added to bring the volume to 5 μL. After incubation for 2 h under visible light, these mixtures were supplemented with 1 μL of 6× gel loading buffer, and loaded into 1% (w/v) agarose gel, prepared with 1× TAE buffer (40 mM Tris-base, 20 mM acetic acid and 1 mM EDTA, pH 8.0). The gel was run at 100 V for 30 min in 1× TAE buffer, and stained with ethidium bromide. The resulting gel was imaged using Gene Genius.

Results and discussion

Characterization of C_{60}–PDA–PEI

The morphological information of the samples was observed by TEM. Fig. S1 (ESI†) shows typical low-magnification images of the pristine C_{60}, in which many nanoplates are stacked together randomly. As the diameter of a single C_{60} is only 0.7 nm, it is very hard to detect and easily forms amorphous aggregates. After modification with PDA, the as-synthesized C_{60}–PDA hybrids existed as cross-linked aggregates with neighbouring ones, as displayed in Fig. 1a as well as an enlarged TEM image in Fig. 1b, and the corresponding energy dispersive X-ray spectroscopy (EDS) (Fig. S2a, ESI†) confirmed the existence of C, O and N elements, which were introduced by PDA. When the hydrophilic polymer PEI was attached to C_{60}–PDA through the Michael addition reaction, the well dispersed C_{60}–PDA–PEI existed as irregular spherical nanoparticles (Fig. 1c). Besides, the diameter of C_{60}–PDA–PEI is about 20–30 nm (Fig. 1d), and the EDS characterization (Fig. S2b, ESI†) proved that the products were also composed of C, O and N elements. These phenomena implied that the introduction of PEI prevented the crosslinking of neighbouring C_{60}–PDA aggregates to a great extent. Meanwhile, C_{60}–PDA–PEI tended to self-assemble in aqueous solution to form uniform nanoparticles with hydrogen bonds, as supported by the dynamic laser scattering (DLS) results. The hydrodynamic size of C_{60}–PDA–PEI nanoparticles

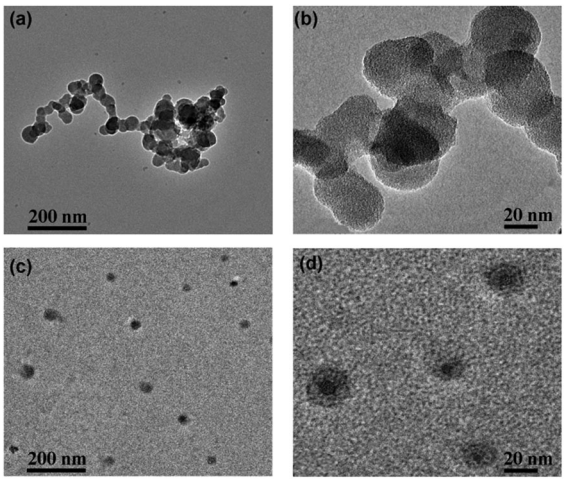

Fig. 1 Representative TEM images of C_{60}–PDA (a and b) and C_{60}–PDA–PEI (c and d) with different magnifications.

in water was 160 nm with a single peak (Fig. S3a, ESI†). This appropriate dimension is feasible for cell uptake. Moreover, the above nanoparticles possess a positive value of ζ potential (41.8 eV) (Fig. S3b, ESI†). Since the cytomembrane is negatively charged, this may be beneficial for their capture by cells *in vivo*. These findings further confirm the C_{60}–PDA–PEI nanoparticles as a candidate for promising materials with biomedical functions.

FT-IR analysis was performed to verify the functionalization of C_{60} in the reaction process. As presented in Fig. 2, distinct peaks at 527, 576, 1187 and 1430 cm^{-1} are the characteristic peaks of pristine C_{60}, which could be related to the three-fold degenerate first-order dipole active T_{1u} modes. Other peaks (2965, 2918 and 1453 cm^{-1}) are the toluene bands and the peak at 3450 cm^{-1} represents the hydroxyl groups of water. After being wrapped by PDA, apart from the 1187 and 1430 cm^{-1} peaks, there were new multiple peaks observed between 1450 and 1600 cm^{-1}, which could be ascribed to the stretching vibration of polycyclic aromatic groups, and the wide band at 3426 cm^{-1} was assigned to the stretching vibration of O–H and

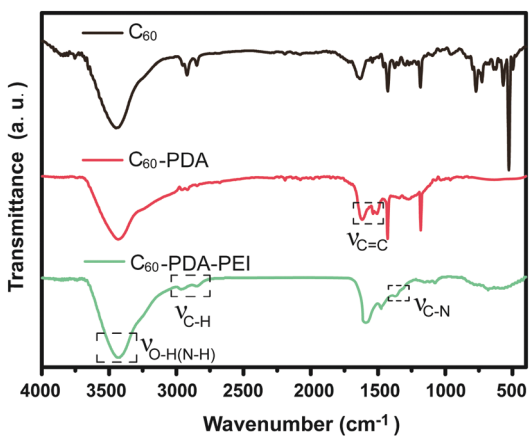

Fig. 2 FT-IR spectra of C_{60}, C_{60}–PDA and C_{60}–PDA–PEI, respectively.

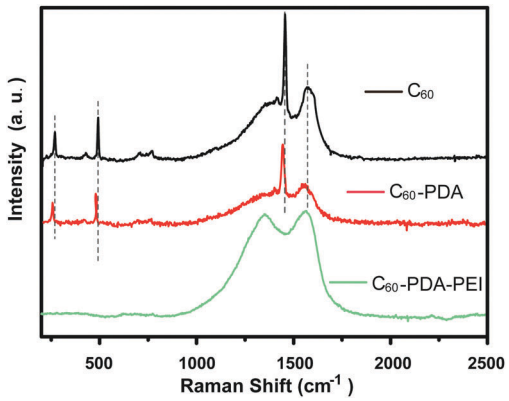

Fig. 3 Raman spectra of C_{60}, C_{60}–PDA and C_{60}–PDA–PEI, respectively.

N–H of PDA, suggesting that C_{60}–PDA was successfully prepared.

Furthermore, several peaks appeared in the spectrum of C_{60}–PDA–PEI compared with C_{60} and C_{60}–PDA. Two peaks at 2935 and 2832 cm^{-1} originated from the stretching vibration of the C–H bond of methylene units, and the stretching vibration of C–N appeared at 1128 cm^{-1}. Meanwhile, the broader and intensive peak around 3430 cm^{-1} could also be attributed to the abundant N–H units of PEI. These observations confirmed that PEI was successfully conjugated with C_{60}–PDA.

Raman spectroscopy has been proven to be a sensitive, local structural probe for carbon nanomaterials and complementary to IR investigation. The Raman spectra of C_{60}, C_{60}–PDA and C_{60}–PDA–PEI are displayed in Fig. 3. For the pristine C_{60}, there are four characteristic peaks, the A_g-breathing mode at 496 cm^{-1}, the A_g-pentagonal pinch mode at 1457 cm^{-1} with two additional H_g modes at 272 cm^{-1} and 1574 cm^{-1}. As for C_{60}–PDA, the typical Raman vibrational frequency of C_{60} was nicely reproduced, evidencing that the structure of the C_{60} cage remained intact after modification with PDA. Notably, all these bands were slightly blue-shifted, presumably due to a vibronic coupling mechanism with electron transfer between C_{60} and PDA.[43,44] Interestingly, in the case of the as-prepared C_{60}–PDA–PEI, the original vibration signals of C_{60} disappeared and two characteristic bands at 1562 and 1352 cm^{-1} appeared. These two bands corresponded to the ordered and disordered carbon structures, respectively, due to the formation of amorphous carbon when grafted by PEI. Specifically, the peak at 1562 cm^{-1} was assigned to the in-plane mode of sp^2 ring vibration (G band, for graphite); while the peak at 1352 cm^{-1} could be assigned as the out of plane mode (D band, for disorder). The above observation was also consistent with our FT-IR findings, revealing that PEI was successfully attached to C_{60}–PDA.

X-ray photoelectron spectroscopy (XPS) was further carried out to characterize the chemical state and composition of the samples. The existence of carbon (C), nitrogen (N) and oxygen (O) elements was revealed, according to the XPS analysis depicted in Fig. 4a, with the survey scan ranging from 0 to 1200 eV, and the high resolution C 1s, N 1s and O 1s XPS

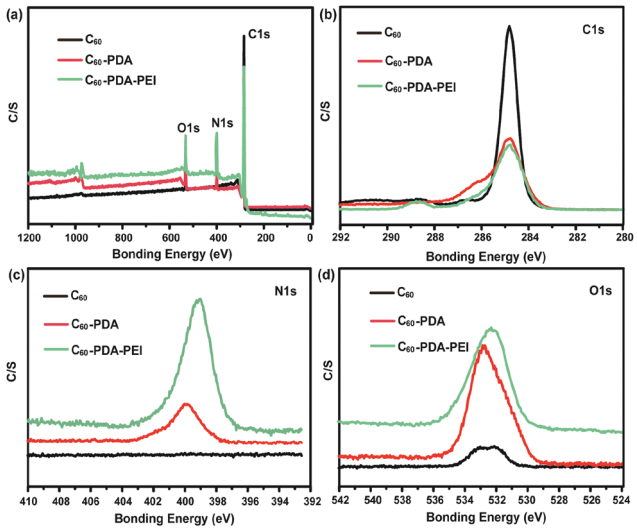

Fig. 4 XPS spectra of C_{60}, C_{60}–PDA and C_{60}–PDA–PEI. (a) Survey scan of the spectral region from 0 to 1200 eV, (b) C 1s region, (c) N 1s region and (d) O 1s region.

spectra can be seen in Fig. 4b–d. The C 1s spectrum of C_{60} contained one symmetrical peak centred at 284.9 eV (Fig. 4b and Fig. S5a, ESI†), which can be assigned to the non-functionalized sp^2-hybridised carbons (C–C and C=C), in good agreement with the spherical symmetry in the electronic structure of the C_{60} molecule. Obviously, there was no nitrogen signal detected for C_{60}. However, after modification with PDA, novel peaks between 285.6–288.4 eV emerged and could be further curve-fitted into two peak components with binding energies at about 287.5 and 286.1 eV, ascribed to the C=O and C–N species, respectively (Fig. S5b, ESI†). More importantly, as can be seen in Fig. 4c, a binding energy peak of C_{60}–PDA of N 1s at 399.9 eV can be attributed to a nitrogen-containing heterocyclic structure formed during the self-polymerization of DA, indicating that PDA was successfully coated on C_{60} *via* mussel inspired chemistry. Furthermore, the marked increase in intensity of the N 1s spectra of C_{60}–PDA–PEI provided strong evidence that PEI was conjugated with C_{60}–PDA through the Michael addition reaction. The peak at 398.8 eV could be related to the amino groups of dopamine and PEI. In addition, the O 1s peaks located between 530 and 535 eV were observed in all the samples (Fig. 4d). With the modification of PDA and PEI, the O 1s peaks were significantly upshifted compared with pristine C_{60}, indicating a higher electron density intensity and consistent with the results of C 1s and N 1s. Besides, the intensity of the O 1s peak in C_{60}–PDA–PEI was a little weaker than that of C_{60}–PDA, which was due to the relatively low content of O in the copolymers. Therefore, the XPS results further confirmed that we could effectively prepare the versatile hybrid polymer modified C_{60} nanoparticles.

The elemental analysis of the C_{60} nanoparticles based on the XPS spectra is listed in Table 1. The major components of pristine C_{60} are C (97.50%) and O (2.50%), which revealed a kind of oxidization without other admixtures. In the case of C_{60}–PDA, the percentages of C and O were altered to 77.41%

Table 1 Element contents (%) of C_{60}, C_{60}–PDA and C_{60}–PDA–PEI based on the XPS analysis

Samples	C 1s	N 1s	O 1s
C_{60}	97.50	0	2.50
C_{60}–PDA	77.41	6.48	16.11
C_{60}–PDA–PEI	71.78	15.05	13.17

and 16.11%, respectively, accompanied with an extra N component (6.48%). The existence of the new element (N) and decrease of C content demonstrated that PDA combined with C_{60} through the strong adhesion of dopamine. After modification of C_{60}–PDA with PEI, the elemental contents of C, N and O in C_{60}–PDA–PEI were 71.78%, 15.05% and 13.17%, respectively. Compared with C_{60} and C_{60}–PDA, an obvious increase in the N content in the sample of C_{60}–PDA–PEI was detected. These results clearly confirmed that PEI was conjugated to C_{60}–PDA through the Michael addition reaction.

Thermogravimetric analysis (TGA) of C_{60}, C_{60}–PDA and C_{60}–PDA–PEI nanoparticles conducted in a nitrogen atmosphere is presented in Fig. 5. As can be noticed, C_{60} was overwhelmingly thermally stable up to 700 °C with only about 4.1% weight loss. However, the total weight loss of functionalized C_{60} with PDA was significantly increased to 30.6% under the same experimental conditions, manifesting that PDA was coated on C_{60} *via* mussel inspired chemistry, thus the relative amount of PDA grafted onto C_{60} was 26.5%, as calculated from the TGA data. When C_{60}–PDA further reacted with the hydrophilic polymer PEI through the Michael addition reaction, much more weight loss was detected in contrast to C_{60}–PDA. The weight loss of C_{60}–PDA–PEI was increased to 59.4%. Consequently, the mass percentage of PEI conjugated to the surface of C_{60}–PDA was calculated to be 32.9%. Based on the above results, we concluded that the amino-containing polymer PEI was indeed grafted to the surface of C_{60}–PDA. The DTA curves of C_{60}, C_{60}–PDA and C_{60}–PDA–PEI are also presented in Fig. S6 (ESI†). For the pristine C_{60}, there was no specific peak but a broad endothermic peak over the whole temperature range could be observed, due to the high thermal-stability of C_{60}. In the case of C_{60}–PDA, a distinct endothermic peak was centred at 560 °C, well consistent with the major weight loss

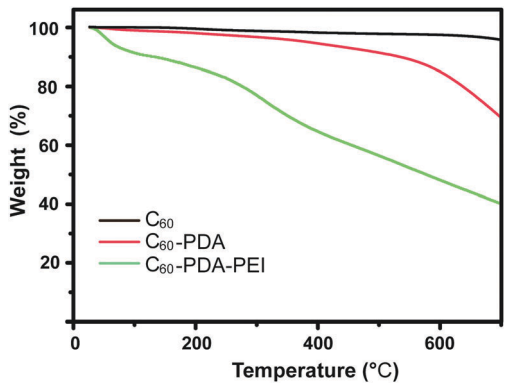

Fig. 5 TGA curves of C_{60}, C_{60}–PDA and C_{60}–PDA–PEI, respectively.

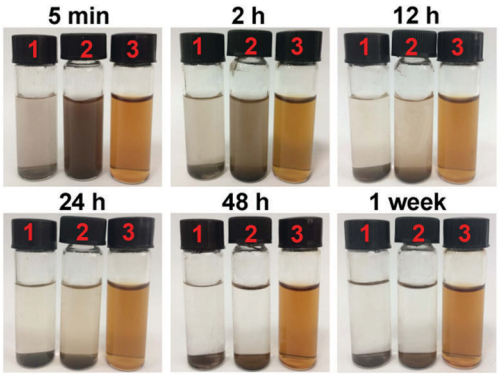

Fig. 6 Optical images of C_{60} (1), C_{60}–PDA (2) and C_{60}–PDA–PEI (3) dispersed in water at room temperature at different times.

range of C_{60}–PDA. Afterwards, two obvious endothermic peaks appeared around 340 and 465 °C in the DTA curve of C_{60}–PDA–PEI, which may be ascribed to the multiple stages of weight loss. These results further confirmed that C_{60} can be facilely modified by PDA and PEI through the combination of mussel inspired chemistry and the Michael addition reaction.

Promoting solubility of functionalized fullerenes is primary and crucial to extend their applications in biological fields. The dispersibility of C_{60} samples in water was then assessed. As illustrated in Fig. 6, the pristine C_{60} precipitated in aqueous solution rapidly within 5 min. With regard to C_{60}–PDA, the water dispersibility was improved a bit, and thus it was deposited in 2 h owing to the finite hydrophilic groups supplied by PDA. In contrast, C_{60}–PDA–PEI nanoparticles exhibited dramatically enhanced dispersibility in water even for a week. Similar results were also confirmed by centrifugation at 8000 rpm for 10 min (Fig. S7, ESI†), implying the high stability of C_{60}–PDA–PEI in aqueous media. These results also demonstrated the successful modification of C_{60} through mussel inspired chemistry and the Michael addition reaction and provided the basis for further biological applications.

To evaluate the photosensitizing ability of C_{60}–PDA–PEI nanoparticles in producing singlet oxygen, the ESR spin-trapping method was carried out under air conditions and irradiation. It is known that pristine C_{60} aggregates do not generate ROS due to the self-quenching of $^3C_{60}$*.[45] As shown in Fig. 7, the distinct signals of TEMPO, a $^1O_2$ adduct of TEMP, clearly confirmed that C_{60}–PDA–PEI nanoparticles well dispersed in the aqueous solution can be excited by visible light irradiation to generate singlet oxygen ($^1O_2$). Such efficient generation of singlet oxygen from C_{60}–PDA–PEI nanoparticles confirms them as a promising phototherapeutic agent in *in vitro* DNA cleaving and further for photodynamic therapy.

Due to the interaction between fullerenes and DNA: direct electron transfer and formation of cytotoxic singlet oxygen species, the water-soluble fullerene derivatives were expected to show high DNA-cleaving activity. Based on the good dispersion of C_{60}–PDA–PEI and efficient $^1O_2$ generation in water, we further evaluated its ability to cleave DNA using pSP72 plasmid as a model. Firstly, the results of control experiments using C_{60}

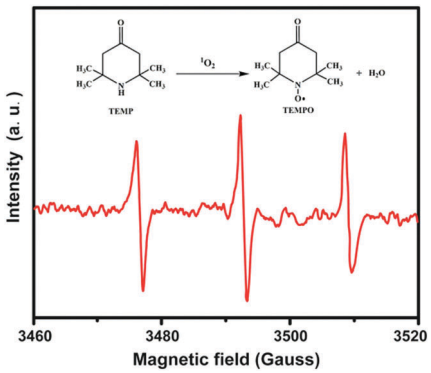

Fig. 7 ESR spectroscopy of TEMP (25 μL, 30 mM) adduct with $^1O_2$ generated in C_{60}–PDA–PEI aqueous solution (25 μL, 0.5 mg mL^{-1}) under irradiation (50 mW cm^{-2}, 10 min).

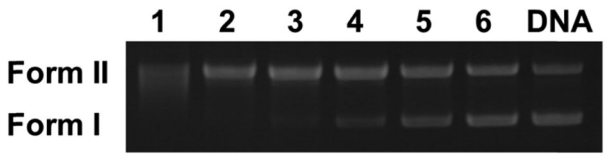

Fig. 8 Agarose gel electrophoresis assay for the pSP72 plasmid DNA in the presence of C_{60}–PDA–PEI under visible light irradiation. The concentration of C_{60}–PDA–PEI for lane 1 was 125 ng μL^{-1} and the concentration was consecutively reduced by half from lane 2 to lane 6. DNA: blank control without addition of C_{60}–PDA–PEI. For all the experiments, the DNA concentration was 25 ng μL^{-1}.

and C_{60}–PDA as references are shown in Fig. S8 (ESI†). In contrast, DNA cleavage was not observed in the presence of hydrophobic C_{60} and C_{60}–PDA. These results were consistent with the previous reports that found that water-solubility of C_{60} is necessary for DNA cleavage.[8,24,46] As displayed in Fig. 8, with increased concentrations of C_{60}–PDA–PEI and under visible light irradiation, supercoiled DNA (Form I) was gradually converted into nicked DNA (Form II), demonstrating the DNA-cleaving ability of C_{60}–PDA–PEI as a photosensitizer. When the concentration was increased to 62.5 ng μL^{-1}, C_{60}–PDA–PEI cleaved DNA completely. Moreover, the smeared bands of nicked DNA were also observed at relatively higher concentrations of C_{60}–PDA–PEI (Lane 1 to 3). In a word, the structural conversions observed above are the results of the DNA strand breaks, indicating that C_{60}–PDA–PEI has a good ability of cleaving DNA upon visible light irradiation.

Conclusions

In conclusion, we have developed a mild strategy to prepare hybrid C_{60}–PDA–PEI nanoparticles by the combination of mussel inspired chemistry and the Michael addition reaction for the first time. The whole process was conducted at normal temperature and pressure without organic solvent, catalysts and initiators, making it truly green, facile and efficient. Incorporation of a quantity of water-soluble groups such as –NH, NH_2 and –OH onto the fullerene core enabled these C_{60} nanoparticles to achieve high dispersibility in aqueous media. As a result, these C_{60}–PDA–PEI nanoparticles with efficient $^1O_2$ generation properties displayed a good ability of cleaving DNA under visible light irradiation, endowing them with promising application potential in photodynamic therapy. Considering the universal adhesion of PDA and abundant second-platforms based on C_{60}–PDA, this achievement could not only provide a new methodology to design and prepare multifunctional fullerene nanoparticles, but also extend the possible applications of fullerene-based species in many fields of pharmaceutical chemistry and biological technology.

Conflicts of interest

There are no conflicts to declare.

Acknowledgements

This research was supported by the National Science Foundation of China (No. 51502352, 21405181 and 51703251), the Fundamental Research Funds for the Central Universities (CZQ 14006) and Beijing National Laboratory for Molecular Sciences.

References

1 C. H. Cui, Y. W. Li and Y. F. Li, *Adv. Energy Mater.*, 2017, **7**, 1601251.
2 S. Goodarzi, T. Da Ros, J. Conde, F. Sefat and M. Mozafari, *Mater. Today*, 2017, **20**, 460–480.
3 L. P. Bao, P. Peng and X. Lu, *Acc. Chem. Res.*, 2018, **51**, 810–815.
4 A. Zieleniewska, F. Lodermeyer, A. Roth and D. M. Guldi, *Chem. Soc. Rev.*, 2018, **47**, 702–714.
5 S. F. Yang, T. Wei and F. Jin, *Chem. Soc. Rev.*, 2017, **46**, 5005–5058.
6 R. Ganesamoorthy, G. Sathiyan and P. Sakthivel, *Sol. Energy Mater. Sol. Cells*, 2017, **161**, 102–148.
7 E. Castro, A. H. Garcia, G. Zavala and L. Echegoyen, *J. Mater. Chem. B*, 2017, **5**, 6523–6535.
8 E. Nakamura, H. Tokuyama, S. Yamago, T. Shiraki and Y. Sugiura, *Bull. Chem. Soc. Jpn.*, 1996, **69**, 2143–2151.
9 P. Mroz, G. P. Tegos, H. Gali, T. Wharton, T. Sarna and M. R. Hamblin, *Photochem. Photobiol. Sci.*, 2007, **6**, 1139–1149.
10 S. K. Sharma, L. Y. Chiang and M. R. Hamblin, *Nanomedicine*, 2011, **6**, 1813–1825.
11 Y. Y. Huang, S. K. Sharma, R. Yin, T. Agrawal, L. Y. Chiang and M. R. Hamblin, *J. Biomed. Nanotechnol.*, 2014, **10**, 1918–1936.
12 I. Rasovic, *Mater. Sci. Technol.*, 2017, **33**, 777–794.
13 X. L. Yang, A. Ebrahimi, J. Li and Q. J. Cui, *Int. J. Nanomed.*, 2014, **9**, 77–92.
14 N. O. McHedlov-Petrossyan, *Chem. Rev.*, 2013, **113**, 5149–5193.

15 K. N. Semenov, N. A. Charykov, V. N. Postnov, V. V. Sharoyko, I. V. Vorotyntsev, M. M. Galagudza and I. V. Murin, *Prog. Solid State Chem.*, 2016, **44**, 59–74.
16 K. N. Semenov, E. V. Andrusenko, N. A. Charykov, E. V. Litasova, G. G. Panova, A. V. Penkova, I. V. Murin and L. B. Piotrovskiy, *Prog. Solid State Chem.*, 2017, **47-48**, 19–36.
17 J. Li, M. R. Guan, T. S. Wang, M. M. Zhen, F. W. Zhao, C. Y. Shu and C. R. Wang, *ACS Appl. Mater. Interfaces*, 2016, **8**, 25770–25776.
18 V. I. Bhoi, S. Kumar and C. N. Murthy, *Carbohydr. Res.*, 2012, **359**, 120–127.
19 L. A. Watanabe, M. P. I. Bhuiyan, B. Jose, T. Kato and N. Nishino, *Tetrahedron Lett.*, 2004, **45**, 7137–7140.
20 Z. L. Yao and K. C. Tam, *Macromol. Rapid Commun.*, 2011, **32**, 1863–1885.
21 S. Oriana, S. Aroua, J. O. B. Sollner, X. J. Ma, Y. Iwamoto and Y. Yamakoshi, *Chem. Commun.*, 2013, **49**, 9302–9304.
22 G. Mountrichas, S. Pispas, E. Xenogiannopoulou, P. Aloukos and S. Couris, *J. Phys. Chem. B*, 2007, **111**, 4315–4319.
23 S. Samal and K. E. Geckeler, *Chem. Commun.*, 2000, 1101–1102.
24 A. Ikeda, Y. Doi, M. Hashizume, J.-i. Kikuchi and T. Konishi, *J. Am. Chem. Soc.*, 2007, **129**, 4140–4141.
25 M. Kovochich, B. Espinasse, M. Auffan, E. M. Hotze, L. Wessel, T. Xia, A. E. Nel and M. R. Wiesner, *Environ. Sci. Technol.*, 2009, **43**, 6378–6384.
26 X. R. Xia, N. A. Monteiro-Riviere and J. E. Riviere, *Toxicol. Lett.*, 2010, **197**, 128–134.
27 A. Ikeda, *J. Inclusion Phenom. Macrocyclic Chem.*, 2013, **77**, 49–65.
28 Y. Nakagawa, T. Suzuki, H. Ishii, D. Nakae and A. Ogata, *Arch. Toxicol.*, 2011, **85**, 1429–1440.
29 H. Lee, S. M. Dellatore, W. M. Miller and P. B. Messersmith, *Science*, 2007, **318**, 426–430.
30 Y. L. Liu, K. L. Ai and L. H. Lu, *Chem. Rev.*, 2014, **114**, 5057–5115.
31 M. Y. Liu, G. J. Zeng, K. Wang, Q. Wan, L. Tao, X. Y. Zhang and Y. Wei, *Nanoscale*, 2016, **8**, 16819–16840.
32 R. Batul, T. Tamanna, A. Khaliq and A. Yu, *Biomater. Sci.*, 2017, **5**, 1204–1229.
33 M. E. Lynge, P. Schattling and B. Stadler, *Nanomedicine*, 2015, **10**, 2725–2742.
34 H. Lee, J. Rho and P. B. Messersmith, *Adv. Mater.*, 2009, **21**, 431–434.
35 J. H. Ryu, P. B. Messersmith and H. Lee, *ACS Appl. Mater. Interfaces*, 2018, **10**, 7523–7540.
36 X. Y. Zhang, M. Y. Liu, Y. L. Zhang, B. Yang, Y. Ji, L. Feng, L. Tao, S. X. Li and Y. Wei, *RSC Adv.*, 2012, **2**, 12153–12155.
37 L. H. Fu, Y. G. Shi, K. Wang, P. Zhou, M. Y. Liu, Q. Wan, L. Tao, X. Y. Zhang and Y. Wei, *New J. Chem.*, 2015, **39**, 8172–8178.
38 Y. G. Shi, M. Y. Liu, K. Wang, F. J. Deng, Q. Wan, Q. Huang, L. H. Fu, X. Y. Zhang and Y. Wei, *Polym. Chem.*, 2015, **6**, 5876–5883.
39 Q. Wan, M. Y. Liu, J. W. Tian, F. J. Deng, G. J. Zeng, Z. Li, K. Wang, Q. S. Zhang, X. Y. Zhang and Y. Wei, *Polym. Chem.*, 2015, **6**, 1786–1792.
40 Q. Wan, L. C. Mao, M. Y. Liu, K. Wang, G. J. Zeng, D. Z. Xu, H. Y. Huang, X. Y. Zhang and Y. Wei, *Polym. Chem.*, 2015, **6**, 7211–7218.
41 X. Y. Zhang, G. J. Zeng, J. W. Tian, Q. Wan, Q. Huang, K. Wang, Q. S. Zhang, M. Y. Liu, F. J. Deng and Y. Wei, *Appl. Surf. Sci.*, 2015, **351**, 425–432.
42 M. Nurunnabi, Z. Khatun, M. Nafiujjaman, D. G. Lee and Y. K. Lee, *ACS Appl. Mater. Interfaces*, 2013, **5**, 8246–8253.
43 F. Negri, G. Orlandi and F. Zerbetto, *Mol. Cryst. Liq. Cryst.*, 1993, **234**, 155–160.
44 L. Zhang, Y. Wang, T. Xu, S. Zhu and Y. Zhu, *J. Mol. Catal. A: Chem.*, 2010, **331**, 7–14.
45 J. Lee, Y. Yamakoshi, J. B. Hughes and J. H. Kim, *Environ. Sci. Technol.*, 2008, **42**, 3459–3464.
46 C. S. Zhou, Q. L. Liu, W. Xu, C. R. Wang and X. H. Fang, *Chem. Commun.*, 2011, **47**, 2982–2984.

